Materials and Design 160 (2018) 1042–1051

Contents lists available at ScienceDirect

Materials and Design

journal homepage: www.elsevier.com/locate/matdes

Enhancing mechanical properties of wire + arc additively manufactured INCONEL 718 superalloy through in-process thermomechanical processing

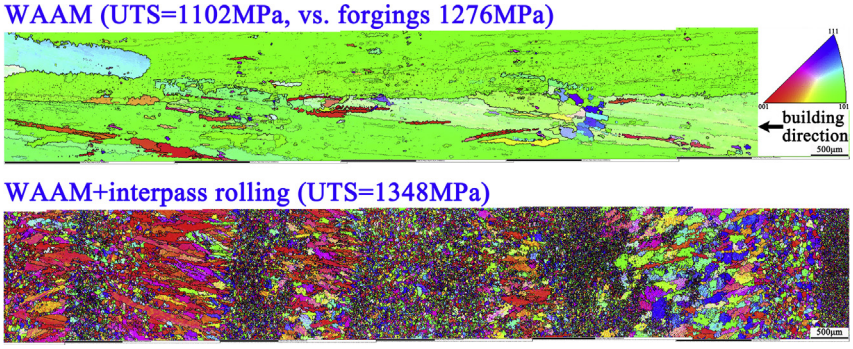
Xiangfang Xu [a,*], Supriyo Ganguly [a], Jialuo Ding [a], Cui Er Seow [b,c], Stewart Williams [a]

[a] Welding Engineering and Laser Processing Centre, Cranfield University, Bedford MK43 0AL, UK
[b] National Structural Integrity Research Centre, Granta Park, Great Abington, Cambridge CB21 6AL, UK
[c] Department of Mechanical Engineering, University of Bristol, Queen's Building, University Walk, Bristol BS8 1TR, UK

HIGHLIGHTS

- Wire + arc additive manufacture (WAAM) was applied to deposit IN718.
- Microstructure and aging response of WAAM IN718 were studied.
- Explanation was given to the inferior strength of WAAM IN718 to the forgings.
- Interpass rolling proved to be effective in enhancing the strength of WAAM IN718.

GRAPHICAL ABSTRACT



ARTICLE INFO

Article history:
Received 5 September 2018
Received in revised form 21 October 2018
Accepted 26 October 2018
Available online 27 October 2018

Keywords:
INCONEL 718
Wire + arc additive manufacture
Thermomechanical processing
Mechanical properties
Recrystallization

ABSTRACT

Wire + arc additive manufacture (WAAM) was applied to produce INCONEL 718 superalloy (IN718) components in a layer by layer manner; further, interpass cold rolling was introduced to generate in-process thermomechanical processing effect during the deposition process. Mechanical testing showed that with rolling applied, the strength of the solution plus aging treated WAAM IN718 was improved from 1056 MPa (unrolled) to 1351 MPa (rolled) which met the wrought standard (1276 MPa), and the material anisotropy was eliminated. The unrolled IN718 featured large columnar grains developing along the building direction, with the length and width as large as 11 mm and 0.8 mm respectively; rolling induced plastic deformation triggered a non-uniform recrystallization upon successive depositions, which produced a recrystallized core with small columnar grains and numerous finely equiaxed grains with the grain size of 12.7 μm. The overall strengthening produced by interpass rolling was attributed mostly (76%) to the rolling induced recrystallization which produced grain size reduction strengthening and created larger grain boundary area to allow more precipitation at the grain boundaries, and partially (24%) due to the improved aging response of the recrystallized grain structure.

© 2018 Elsevier Ltd. This is an open access article under the CC BY-NC-ND license (http://creativecommons.org/licenses/by-nc-nd/4.0/).

1. Introduction

INCONEL 718 superalloy (IN718) is a precipitation hardenable Ni-based alloy outstanding for its capability of retaining mechanical properties at elevated temperatures [1]. The combination of excellent tensile

* Corresponding author.
E-mail address: xiangfang.xu@cranfield.ac.uk (X. Xu).

https://doi.org/10.1016/j.matdes.2018.10.038
0264-1275/© 2018 Elsevier Ltd. This is an open access article under the CC BY-NC-ND license (http://creativecommons.org/licenses/by-nc-nd/4.0/).

and creep strength, corrosion resistance, and weldability makes IN718 the most widely used superalloy in today's turbine engine applications, accounting for 55–70% of the Ni-base superalloys in modern jet engines [2] and >30% of the total weight [3].

IN718 gains high strength through the precipitation of a wide variety of secondary phases into the austenitic matrix (γ phase). The most common secondary phases include γ″ (Ni_3Nb, ordered bct $D0_{22}$ structure), γ′ ($Ni_3(Al,Ti)$, $L1_2$ structure) and metal carbides. In terms of volume (16% [3]) and influence, the primary strengthening phase is γ″, a lens-like disc-shaped/needle-shaped precipitate with the size of 30–50 nm; besides, a small volume fraction (4%vol. [3]) of γ′, a cubic or spherically shaped precipitate with the size of 50–100 nm [4], is also reported to affect the microstructure stability [5]. If the hardening constituents are precipitated as other phases or are combined in other forms, the full strength of IN718 will not be attained [6]; therefore other phases such as Laves phase and δ phase (Ni_3Nb, orthorhombic) which form due to the variations in composition, processing or high-temperature exposure [7], are undesirable.

IN718 is an expensive alloy and the machining remains a challenge. The inherent characteristics, such as the high work hardening rate, low thermal conductivity, adherence to the cutting edge and presence of abrasive carbides, make the machining difficult since the high temperature and stress are generated at the tool-workpiece interface to result in short tool life and metallurgical damage to the workpiece [8]. Therefore, cost-effective manufacturing methods are required to reduce material wastage and ease the machining process. Metal additive manufacture (AM) [9] provides the above benefits by building near-net-shape components in a layer by layer manner. So far, the AM research on IN718 is mainly focused on various laser-powder processes: the powder bed fusion process could produce IN718 with equivalent or superior mechanical properties than the wrought alloy due to the fast cooling rate induced fine grains [1,10]; while the blown powder process produced IN718 with comparable or slightly inferior strength [3,11] due to the relatively high heat input. However, the laser-powder AM parts were frequently associated with unmelted powder particles [12] and porosity issues [13]. Anisotropy was observed such that the samples extracted along the horizontal direction were characterized by a higher ultimate tensile strength (UTS, 1440 MPa vs. 1400 MPa) and a lower elongation (18.5% against 20.4%) due to the layered structure [10].

Wire + arc additive manufacture (WAAM) [14], which adopts an electric arc as the heat source and a commercial welding wire as the feedstock [15–17], is outstanding for its low equipment cost, high building rate and large-scale (meters scale) product. In contrast to the laser-powder based AM process, there is very little research on WAAM of IN718. So far, limited trials have been carried out using the tungsten inert gas (TIG) [2,18] or the metal inert gas (MIG) [19] which prove the feasibility to deposit simple features using WAAM; however, plasma arc has not been applied to deposit IN718 and the heat treatment response of the WAAM IN718 is yet to be studied.

In this paper, the plasma arc based WAAM process was applied to produce IN718 components and a complete microstructure and mechanical properties study was carried out to understand the relationship between the WAAM microstructure and the macro properties. Furthermore, in-process interpass rolling was applied to the layer by layer deposition process, aiming to improve the microstructure of the WAAM IN718 and thereby the mechanical properties to the level comparable to the wrought alloy.

2. Experimental

2.1. Rolling-WAAM system and deposition procedure

The in-process thermomechanical processing assisted WAAM process is realized by integrating two subsystems: WAAM deposition system and cold rolling system [20], as shown in Fig. 1a. The former deploys a plasma arc (power source: Fronius TransTig 5000 + A-4600 Wels PlasmaModule 10) as the heat source, and a 3-axis CNC gantry system is used to control the deposition path. The chemical composition of the 1.2 mm IN718 wire is listed in Table 1. A laminar flow local shielding device developed at Cranfield University [21] is attached around the torch to provide additional shielding to the deposits (purified Ar, flow rate 200 l/min). The latter consists of a rigid flat roller (diameter 100 mm, width 20 mm) and a hydraulic cylinder through which the force could be loaded to induce plastic deformation in the top deposit;

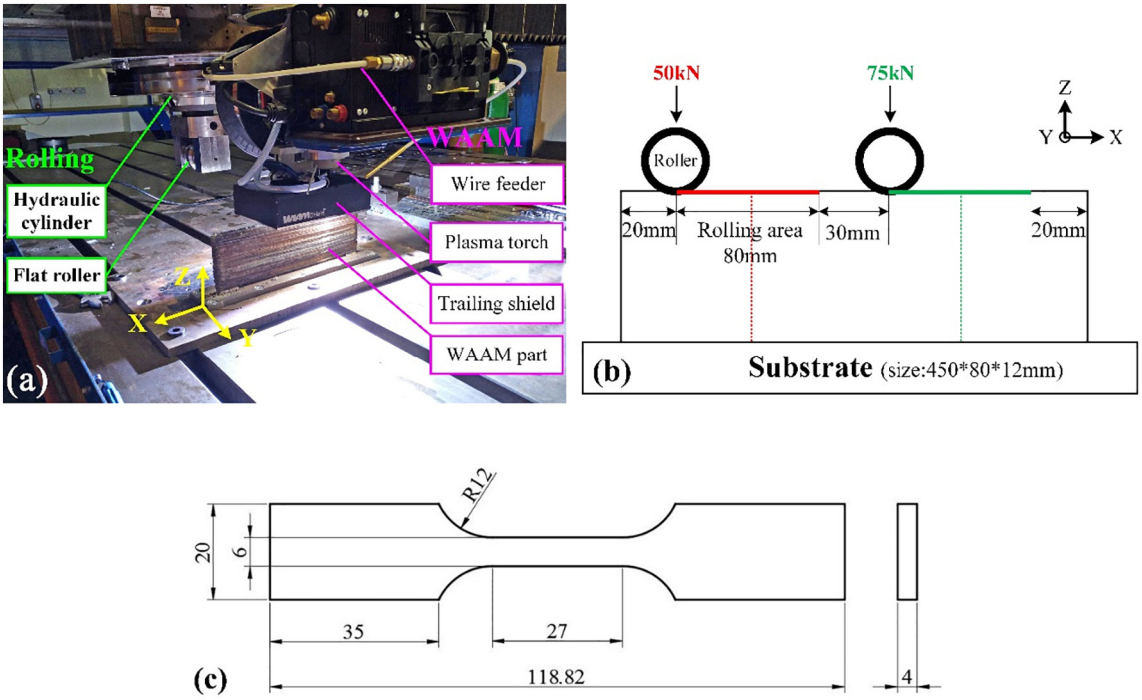


Fig. 1. (a) Experimental setup of the in-process rolling assisted WAAM system and (b) principle of one pass rolling study (c) dimensions of the tensile specimens (note that the 27 mm is the parallel length).

Table 1
Chemical composition of the IN718 wire (wt%).

Ni	Cr	Nb + Ta	Mo	Ti	Al	Co	Mn	Fe
53.15	19.42	5.22	2.95	0.96	0.47	0.41	0.11	Bal.

the motion of the rolling system is controlled by the same CNC system and is aligned with the deposition path.

To study the effect of an individual rolling pass on the deposit, a 5-layer single pass wall structure was deposited, then only the top deposit was applied one pass of cold rolling with 50 kN and 75 kN respectively, as shown in Fig. 1b. To evaluate the overall effectiveness of rolling on improving the mechanical properties of WAAM IN718, two comparative linear wall structures (length: 400 mm, height: 134 mm) were deposited: the first was deposited in a normal layer-by-layer manner; while the second was applied 75 kN interpass cold rolling (hereinafter, rolling or rolled), i.e., rolling and deposition took place in turns so that the deposition was always on a plastically deformed deposit. Each rolling was applied 2 min after the deposition finished. All the depositions were along X axis (see Fig. 1a). The process parameters were kept consistent: contact tip-to-work distance (CTWD) = 8 mm, current = 180 A, wire feed speed (WFS) = 4 m/min, torch travel speed (TS) = 7.5 m/min, roller travel speed 2 m/min, plasma Ar flow rate = 0.8 l/min, shielding Ar flow rate = 10 l/min, and interpass cooling time = 3 min.

2.2. Mechanical testing and microstructural analysis

The heat treatment conforming to Aerospace Material Specifications (AMS-5662M, for forged IN718) was applied to the WAAM IN718: solution treatment at 970 °C for 1 h, water quenching; aging at 718 °C, hold for 8 h; furnace cool to 620 °C, hold for 8 h, air cool (hereinafter, solution plus aging treatment). The tensile specimens were extracted along both horizontal (X) and vertical (Z) directions using the material leaving out 10 mm from both ends and 10 mm from the top and the substrate, and the tensile specimen design conforming to BS EN 2002-1: 2005 standard is shown in Fig. 1c. The room temperature mechanical testing was carried out on the Instron 5500R Electro-mechanical machine with a load cell of 100 kN and a crosshead speed of 1 mm/min, and at least three samples were tested for each condition; the elongation was measured through a laser extensometer using a gauge length of 24 mm.

The samples for microstructural analysis underwent a metallographic preparation consisting of mounting, grinding and polishing. The microstructure was revealed by electrolytic etching in the 10% oxalic acid solution using 6 V for 10 s. The grain size was determined using the line intercept method [22]. The microhardness was measured using a Zwick/Roell hardness tester under a load of 1 kg and holding time of 15 s. The optical microscope and scanning electron microscopy (SEM, FEI XL30-SFEG) were used to observe the precipitates. The phase identification was carried out using X-ray diffraction (SIEMENS D5005) with Cu Kα radiation (λ = 1.5418 Å). The grain structure was characterized by electron backscatter diffraction (EBSD) analysis. In parallel, a piece of wrought IN718 (HAYNES® 718 alloy) conforming to the AMS 5596 specification was prepared and underwent the same heat treatment and analysis for a comparative study.

3. Results

3.1. Microhardness

Fig. 2 shows the microhardness variation of the one-pass and interpass rolled wall structures measured from the top to the bottom along the central axis of the YZ plane. The sample sectioning positions are indicated by the dash lines in Fig. 1b. From Fig. 2a, with one pass rolling a noticeable hardness increase is observed near the top and the hardening depth could reach 5 mm. Hardening occurs instantly from the top surface, gets more pronounced to reach the peak value at 1.6–2.2 mm depth, then reduces all the way till the unhardened level. Generally, the higher the load, the higher microhardness value at the same depth; the peak microhardness obtained after 50 kN and 75 kN rolling is 324 HV and 355 HV respectively, as compared to the 230 HV of the unhardened level.

Fig. 2b presents the microhardness variations of the two comparative walls built with and without rolling. In the as deposited condition, the microhardness generally remains a constant level from the top to the substrate despite the slight fluctuation, indicating a very sluggish response of IN718 to the intrinsic aging effect [23,24] from the layer-by-layer deposition process. With rolling applied, the WAAM IN718 shows a considerable hardness increase of 71 HV in the as deposited condition. After solution plus aging treatment, the microhardness value of both unrolled and rolled alloy shows a significant increase of 158 HV and 113 HV respectively, and the rolled alloy still shows a slightly higher (26 HV) microhardness than the unrolled one.

3.2. Macrostructure

Fig. 3 shows the macrostructure of the unrolled and rolled WAAM IN718 along the YZ plane. The sequentially appeared remelting lines (yellow dotted lines in Fig. 3) indicate the layer by layer building principle in which the subsequent depositions partially remelt the previous one and solidifies on the top to form a new layer. The unrolled alloy exhibits a typical solidified dendritic structure: large columnar grains are observed to grow along the wall height and could cross several layers with the lengths comparable to the wall height. By contrast, the rolled alloy exhibits a duplex grain structure with a recrystallized core in the central area covering half the wall thickness and smaller columnar grains located near the wall sides. Note that the tensile specimens are extracted along the XZ plane and in the central area of the thickness, i.e., in the fully recrystallized area. Although the columnar grains show

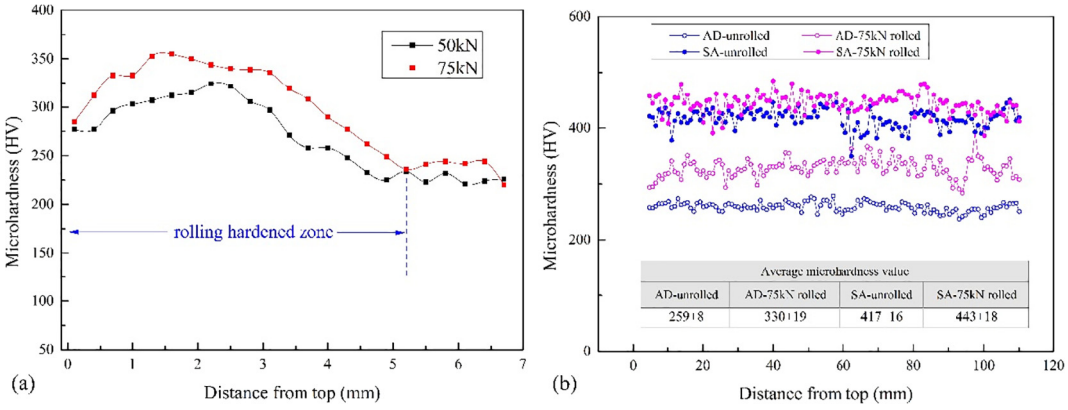


Fig. 2. Microhardness of the wall built with (a) one pass rolling on top and (b) interpass rolling (AD: as deposited; SA: solution plus aging treated).

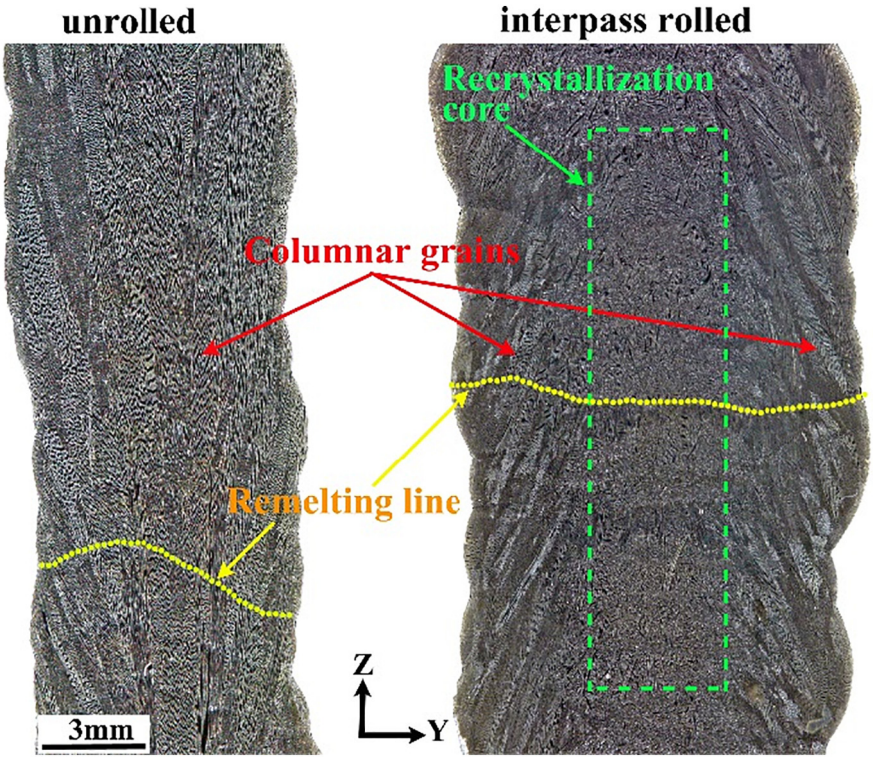


Fig. 3. Macrostructure of the unrolled and rolled WAAM IN718. (Images taken near the top of the wall, covering 1/4 of the wall height.)

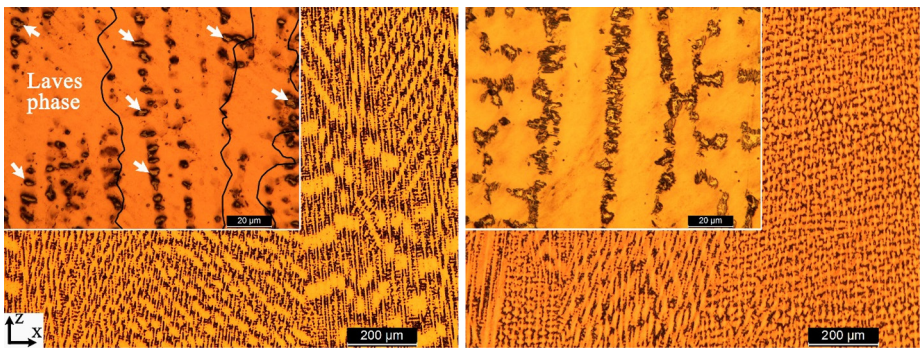
different orientations such that they grow divergently upwards in the unrolled alloy but convergently upwards in the rolled one, they both show an epitaxial growth in a direction perpendicular to the remelting line.

3.3. Microstructure

Figs. 4 and 5 show the microstructure of the unrolled and rolled WAAM IN718 respectively. The micrographs were taken at the half height of the wall. In the as deposited condition, the unrolled WAAM IN718 (Fig. 4a) exhibits a dendritic structure with the dendrites developing along the building direction (Z); numerous Laves phase (white arrows in Fig. 4a) are observed to distribute in the interdendritic regions. After solution plus aging treatment, the dendritic microstructure generally remains unchanged, but a higher magnification shows that some Laves phase particles are dissolved through the thermodynamic diffusion process and the amount of Laves phase is reduced (Fig. 4b). When rolling is applied (Fig. 5a), the microstructure is less dendritic and dendrite growth direction within each layer is more random compared to that of the rolled material; particularly, the long dendrites do not necessarily grow perpendicularly to the interlayer boundary. With solution plus aging treatment applied, the similar diffusion and reduction of Laves phase are observed (Fig. 5b), and the secondary phase particles are more evenly distributed as compared to the unrolled alloy (Fig. 4b).

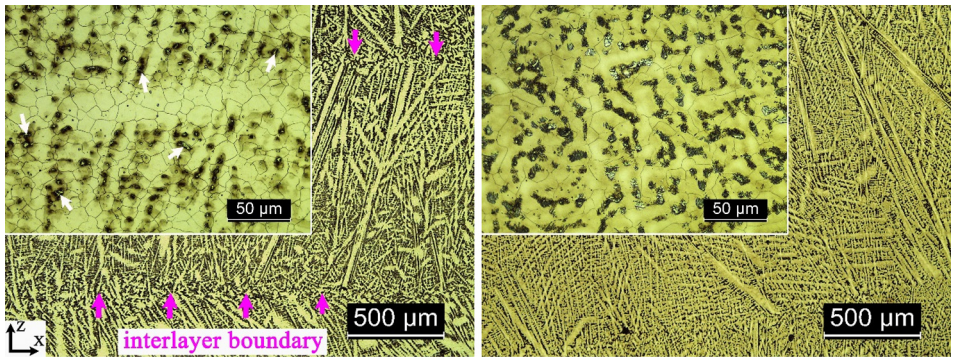
3.4. Mechanical testing results

Table 2 presents the tensile test results of the unrolled and rolled WAAM IN718 under different heat treatment conditions. Without rolling, the average UTS of the as deposited WAAM IN718 is 793 MPa, and with rolling only applied the UTS is increased to 1078 MPa (increased by 35.9%) which is accompanied by a 7.1% elongation reduction in the horizontal direction. A full heat treatment, solution plus aging, of the unrolled WAAM IN718 improved the UTS to 1056 MPa (increased by 33.2%), which is essentially the same efficacy as rolling only does,



(a) as deposited (grain boundary depicted for better visibility) (b) solution plus aging treated

Fig. 4. Microstructure of the unrolled WAAM IN718.



(a) as deposited (b) solution plus aging treated

Fig. 5. Microstructure of the rolled WAAM IN718.

except that the elongation is only around half of that resulted from rolling only; however, the UTS is still 220 MPa lower than the wrought standard (1276 MPa). Solution treatment results in a UTS reduction of 58 MPa and 118 MPa for the unrolled and rolled alloys respectively, which indicates that the rolled alloy responds to the intrinsic aging effect [25,26] more effectively; however, the UTS of the rolled alloy is still 225 MPa higher than the unrolled alloy. After solution plus aging treatment, the UTS of the rolled alloy is improved from 1078 MPa to 1351 MPa (increased by 25.3%) which meets the wrought standard; besides, both the 0.2% yield strength (0.2%YS) and elongation meet the wrought standard.

From Table 2, the elongation generally increases after solution treatment except for the unrolled alloy in the horizontal direction but reduces after aging yet still exceeding the wrought level (12%). This is because the precipitates produced through aging hinder the dislocation motion, which increases the strength and reduces the ductility at the same time. The precipitates formed in the as deposited alloy in response to the WAAM thermal history are dissolved after solutionizing, hence the increase in elongation. Compared with the unrolled alloy, the rolled alloy shows a higher ductility in both solution and solution plus aging treated condition but slightly lower ductility in the as deposited condition.

4. Discussion

4.1. Recrystallization

4.1.1. Duplex grain structure

The duplex grain structure in Fig. 3 indicates that the recrystallization during the rolling assisted WAAM process is not spatially complete, which is related to the non-uniform hardening distribution from an individual rolling pass when using the flat roller, as shown in Fig. 6. As can be seen, one pass of rolling can generate a noticeable hardening zone which is near the central axis of the wall thickness, covering around half of the thickness and a depth of nearly 5 mm from the rolling surface; the material does not get hardened significantly outside this zone. Actually, the material outside this zone will never get hardened even during the entire interpass rolling assisted WAAM process because the rolling load applied in this study is unidirectionally along Z, rather than in all directions. The peak hardening zone (red color in Fig. 6) is not right at the top but at an area 0.5–2.5 mm below the top and 0.5–2.5 mm away from the central axis. The peak hardening point possesses a value that is almost double of the non-deformed material. Since the stored energy induced by rolling provides the thermodynamic driving force to trigger recrystallization [27,28], the hardened zone in the central area shows a more pronounced recrystallization as compared to the area outside it, thus resulting in the duplex grain structure.

4.1.2. Effective rolling for recrystallization

The above correlation of the hardened zone and the recrystallized core indicates that the material being hardened is the prerequisite for recrystallization to take place. Another key element to trigger recrystallization is that the strained material must be heated up to the recrystallization temperature range, but not the melting range. Hence the relationship between the rolling hardened depth and the remelting depth upon next deposition is crucial: the former must be greater than the latter to allow some strained material to be heated up to the temperature just below liquidus; if the other way around, all the strained material will be fully melted and the deposit will only be a normal solidified dendritic structure, without any recrystallization.

Owing to the fcc crystal structure and the high work hardening coefficient [8] of IN718, each individual rolling pass can be so effective that the appreciable hardening depth can be as great as 5 mm, while the remelting depth is below 1.2 mm (layer height in this study). As a result, around 80% of the hardened material remains below solidus and is subject to high temperature upon next deposition, which provides the two key elements for recrystallization to happen. Such recrystallization is not a uniform one for the following reasons. Firstly, the level of recrystallization is strongly dependent on the stored energy; while the strain hardening at a certain position could be partially released by the heat

Table 2
Mechanical testing results of WAAM IN718.

			UTS/MPa			0.2%YS/MPa		Elongation/%	
			H	V	Average	H	V	H	V
WAAM	AD	Unrolled	818 ± 13	756 ± 7	793 ± 32	525 ± 7	506 ± 2	33.3 ± 2.5	27.9 ± 1.3
		75 kN rolled	1082 ± 13	1072 ± 6	1078 ± 12	763 ± 8	687 ± 1	26.2 ± 2.2	26.6 ± 1.3
	S	Unrolled	763 ± 32	693 ± 0	735 ± 42	384 ± 8	384 ± 11	24.4 ± 3.7	32.5 ± 3.0
		75 kN rolled	967 ± 8	949 ± 11	960 ± 13	540 ± 13	530 ± 6	37.0 ± 2.1	32.8 ± 1.0
	SA	Unrolled	1102 ± 78	988 ± 6	1056 ± 82	790 ± 9	791 ± 14	14.7 ± 1.3	12.8 ± 1.2
		75 kN rolled	1348 ± 10	1356 ± 10	1351 ± 11	1057 ± 19	1035 ± 20	15.1 ± 3.3	17.4 ± 1.1
Wrought AMS5662 [3]			1276			1034		12	

AD: as deposited; S: solution treated; SA: solution plus aging treated; H: horizontal; V: vertical.

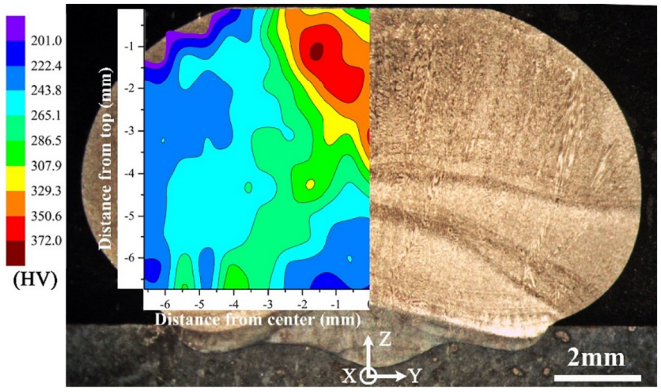


Fig. 6. Microhardness mapping of the 75 kN one-pass top rolled 5-layer wall structure (note: measurement starts from the central top in a matrix form; interval of the indentation points: 0.6 mm).

input from the following depositions and recrystallization process and could also be enhanced upon the following rolling passes. Secondly, the recrystallization temperature is not kept at a constant value but in the form of thermal pulses; also, the fast cooling rate does not leave enough time to allow the recrystallization to proceed thoroughly, and any successive depositions that can heat the strained material to recrystallization temperature would promote the recrystallization process. Thirdly, the growth of the recrystallized grains is subject to non-uniform thermal pulses and discrete duration periods; thereby being unpredicted. The entire rolling assisted WAAM process is essentially an ongoing "deposition-non-uniform recrystallization" pattern.

4.2. Grain morphology, grain size, and texture

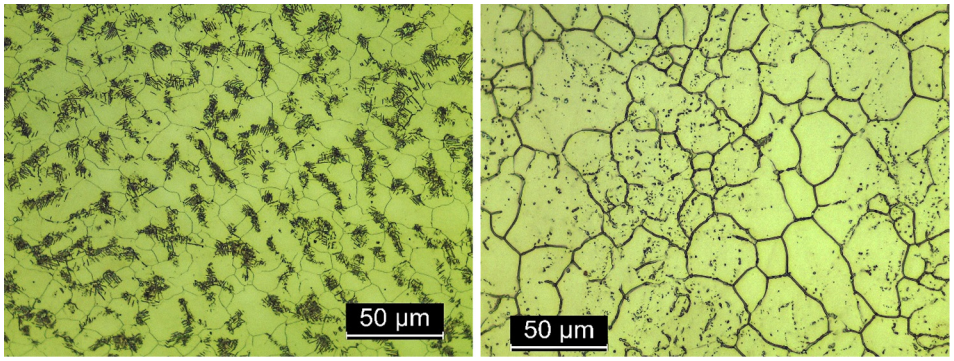
The insets in Figs. 4a and 5a also show the grain boundary morphology of the unrolled and rolled WAAM IN718 in the as deposited condition. The unrolled alloy features low-angle grain boundaries showing the columnar grains (Fig. 4a), while the rolled alloy shows a finely recrystallized equiaxed grains with an average grain size of 12.7 μm. Fig. 7 shows the grain morphology of the rolled WAAM IN718 and the wrought IN718 in the solution treated condition which are also the respective starting microstructure of the following aging treatment. The elemental segregation is more severe in the WAAM alloy as compared to the wrought alloy. The average grain size of the rolled WAAM IN718 is measured to be 15.7 μm, which is slightly larger than the as deposited condition due to the slight grain growth during solution treatment. However, the size of the fully recrystallized grains is still finer than the wrought alloy (26.7 μm, data from the specification sheet) possibly because the fast cooling rate in WAAM deposition, which is essentially a micro casting process, does not allow enough time for the grain growth, whereas the grains in the wrought alloy develop from conventional castings which possess much bigger starting grains.

Fig. 8 presents the EBSD orientation maps for both the unrolled and rolled WAAM IN718 in the solution plus aging treated condition showing their respective grain morphology. In the unrolled alloy, very large columnar grains are observed to extend along the wall height direction (Z). The length of the columnar grains can be >11 mm and the width could be >0.8 mm (Fig. 8a). In addition, the majority of the crystals in the unrolled alloy show a preferred {101} orientation, indicating that the material is strongly textured. By contrast, the EBSD map of the rolled WAAM IN718 shows an overall non-uniformly recrystallized grain structure consisting of alternating bands of finely equiaxed grains and small columnar grains in between the bands (Fig. 8b). The overall grain size is smaller and the texture is weaker than the unrolled WAAM material. Fig. 9a shows a typical area in Fig. 8b. As can be seen, the finely equiaxed grains in the alternating bands are randomly oriented, while the small columnar grains in between the bands are moderately textured with a preferred {100} orientation. The bands of finely equiaxed grains are likely to correspond to the areas which have undergone more thermal cycles, i.e. the remelted zones in between the deposited layers (interlayer boundaries as shown in Fig. 5a). The repeated thermal cycling enables the grains in these areas to become fully recrystallized, giving rise to the present characteristic microstructure. Between these bands are larger columnar grains, which are likely to have resulted from the lack of sufficient thermal cycling for recrystallization. Despite this, in comparison with the unrolled alloy, the size of the columnar grains in the rolled material is significantly smaller in both width (<0.1 mm) and length (<1 mm). Though the recrystallized area accounts for >50% in Fig. 8b, the grain structure of the rolled WAAM IN718 is not improved to a level identical to the wrought alloy (Fig. 9b).

Another benefit from recrystallization is the mitigation of texture. From Table 2, the unrolled WAAM IN718 shows a noticeable anisotropy with the UTS difference between the horizontal and vertical direction being 114 MPa in the solution plus aging treated condition, which is due to the strong {100} texture showing an intensity of 45.05 times more random (Fig. 10a). By contrast, the rolled WAAM IN718 shows an intensity of only 5.51 (Fig. 10b), which is close to the wrought alloy of 2.7 (Fig. 10c). The significant texture weakening is responsible for the essential isotropic mechanical properties of the rolled WAAM IN718 in which the UTS difference is only 8 MPa in the solution plus aging treated condition.

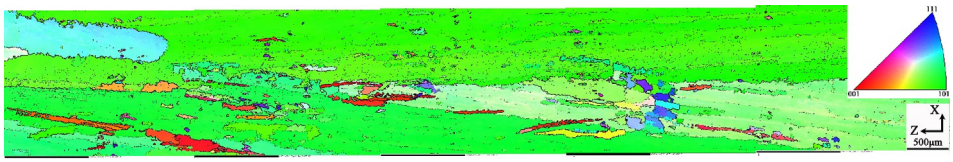
4.3. Precipitates

Fig. 11 shows the X-ray diffraction patterns and the phase index results of the IN718 produced by WAAM and wrought process. The peak

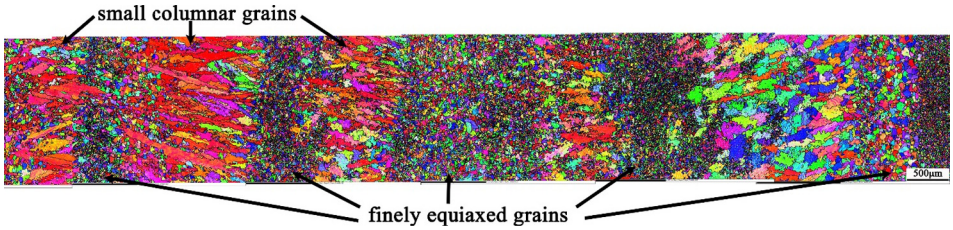


(a) rolled WAAM (b) wrought

Fig. 7. Grain morphology of the rolled WAAM and wrought IN718 after solution treatment.



(a) unrolled



(b) rolled

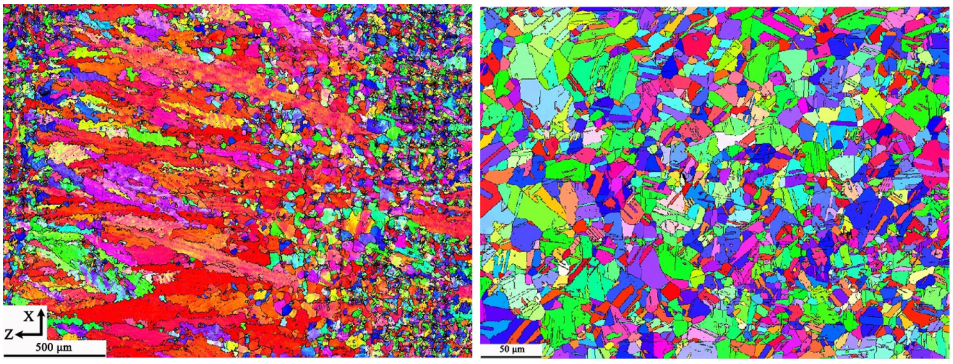
Fig. 8. EBSD orientation maps of the WAAM IN718 after solution plus aging treatment (IPF X; black lines are grain boundaries with misorientation greater than 15°).

of the δ phase appears after heat treating the rolled WAAM IN718, but not in the wrought alloy. The typical (111) and (200) peaks for the γ matrix is very insignificant in the as deposited unrolled WAAM IN718 and they even disappear after solution plus aging treatment, which is likely due to the considerable texture of the unrolled WAAM alloy as shown in Fig. 10a. Peaks of γ′ and γ″ are not detected due to the very fine nature of these precipitates [29].

Fig. 12a shows the morphology and distribution of the precipitates formed in the unrolled WAAM IN718 after solution plus aging treatment. Discrete islands of residual Laves phase are still present since the solution treatment does not dissolve all the Laves phase [3]; besides, a large number of acicular δ phase is observed and generally clusters near the residual Laves phase. Rolling does not eliminate the Laves phase, and both residual Laves phase and δ phase are observed in the rolled alloy after solution plus aging, as shown in Fig. 12b; however, despite the complexity of the precipitates, some nanoscale secondary phases are observed to precipitate at the grain boundaries. Neither Laves phase nor large acicular δ phase is found in the wrought alloy, and the precipitates formed in the wrought alloy are all in nanoscale which disperse very uniformly throughout the austenitic matrix and preferentially precipitate along the grain boundaries.

4.4. Strengthening mechanism

WAAM is a manufacturing process which accumulates material by solidifying the melted droplet, therefore the WAAM alloy is essentially a solidified freeform structure featuring dendritic microstructure. The inherent dendrites growth and non-equilibrium thermal history in WAAM process inevitably result in the Nb segregation and formation of Nb-rich brittle Laves phase at the interdendritic area, which is known to be detrimental to mechanical properties of IN718 [30]. Besides, the directional thermal conduction route in WAAM process also promotes epitaxial growth of the dendrites, which facilitates the development of very big columnar grains, as shown in Fig. 8a. Big columnar grains, on the one hand, provide less effective grain boundary strengthening according to the Hall-Petch relationship [31]; on the other hand, possess less grain boundary area to allow precipitation at the grain boundary. Solution treatment does not dissolve all the Laves phase since the solution temperature of 980 °C is not high enough to promote a complete Nb diffusion, therefore some residual Laves phase still presents in the heat treated WAAM IN718 (Fig. 12a). Homogenization (1093 °C, 1–2 h) using a higher temperature is reported to completely dissolve the Laves phase but results in grain coarsening at the same



(a) WAAM-rolled (b) wrought

Fig. 9. EBSD orientation maps of IN718 produced by different process after solution plus aging (IPF X; black lines are grain boundaries with misorientation greater than 15°).

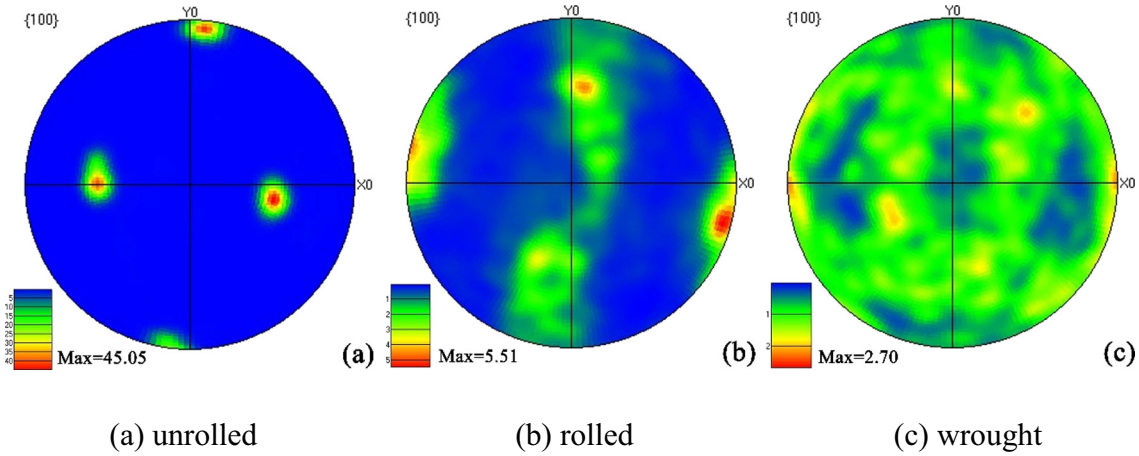


Fig. 10. Pole figures showing the texture of the IN718 in solution plus aging treated condition.

time [3]. Hence, the unrolled WAAM IN718 possesses inferior mechanical properties mostly due to the large columnar grains featured microstructure, which cannot be improved simply by a different heat treatment without introducing plastic deformation.

During the manufacturing process, the wrought IN718 undergoes several rounds of rolling and heating-cooling cycles. Undesired Laves phase can be completely dissolved by heating up to the homogenization temperature, and the resultant grain coarsening can be restored through several rounds of recrystallization which end up with finely equiaxed grains. Besides, the large grain boundary area allows numerous nanoscale secondary phases to precipitate at the grain boundary, as shown in Fig. 12c, which is effective in hindering the grain boundary motion.

Similarly, the rolling applied in this study plays the same role. However, due to the same solution temperature, the Laves phase formed after deposition is not completely dissolved to saturate the matrix with Nb and the residual Laves phase is also observed in the rolled alloy (see green arrows in Fig. 12b); instead, the Laves phase is in situ transformed to acicular δ phase, which depletes the Nb required for γ″ formation [3]. This is the reason why the aging response of the unrolled and rolled alloy are not very different (321 MPa vs. 391 MPa). Thus, the main strengthening mechanism, when comparing the unrolled and rolled WAAM IN718 in the solution plus aging treated condition, is recrystallization. On the one hand, the average grain size in the recrystallized core is 17.6 μm after solution plus aging treatment (Fig. 5b), which is significantly smaller than the centimeter scale columnar grains in the unrolled alloy (Fig. 5a) and thereby having a much greater grain boundary strengthening effect. On the other hand, the grain size is even smaller than the wrought alloy, thereby providing a larger grain boundary area for the precipitation at the grain boundaries, as shown in Fig. 12b.

To conclude, the strength inferiority of the unrolled alloy to the wrought alloy is mostly due to the undesired large columnar grains providing less grain boundary strengthening. The applied rolling is effective because it restores the grain size to somewhere close to the wrought alloy by inducing recrystallization.

4.5. Strengthening contribution

From Table 2, the precipitation hardened rolled alloy shows a strength 295 MPa higher than the unrolled alloy. Such a strengthening after interpass rolling is applied could be a synergic effect of recrystallization and precipitation hardening. Though it is difficult to precisely specify the contribution of each strengthening mechanism, a semi-quantitative discussion can be given here.

The UTS difference in the as deposited condition is 285 MPa, which is a consequence of recrystallization and the intrinsic aging effect. Note that the precipitates formed in response to the intrinsic aging effect will be dissolved and slight grain coarsening might take place during solution treatment. From Figs. 5a and 7a, the average grain size increases from 12.7 μm to 15.7 μm after solution treatment, which is not a significant coarsening. Therefore, by comparing the UTS in the solution treated condition it can be inferred that for the entire 285 MPa increase, the grain structure change contributes to slightly >225 MPa and the better intrinsic aging response of the rolled grain structure contributes to around 60 MPa.

Further, when aging is applied, the strength increase is 321 MPa and 391 MPa for the unrolled and rolled WAAM IN718 respectively, which indicates that the aging response of the unrolled grain structure is 70 MPa lower than the rolled grain structure. Again, a slight grain coarsening, from 15.7 μm to 17.6 μm, is observed after the double aging treatment. Hence, for the overall 295 MPa strength increase in the solution plus aging treated condition, grain structure change contributes slightly <225 MPa (76%), and the better aging response from the recrystallized grain structure contributes to the remaining, around 70 MPa (24%).

4.6. Future work

From this paper, although interpass rolling improves the mechanical properties of the WAAM IN718 to a level superior to the wrought alloy, it does not make the WAAM alloy microstructurally and metallurgically identical to a wrought alloy. Firstly, the rolling induced recrystallization is not spatially uniform and some area remains columnar grains with

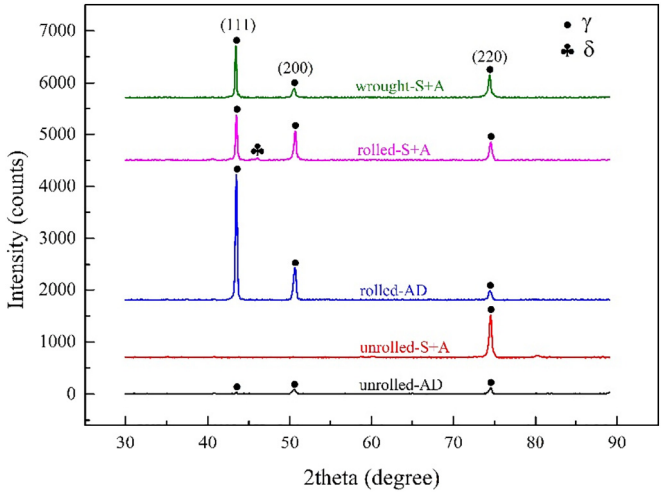


Fig. 11. X-ray diffraction patterns of IN718 produced by different process.

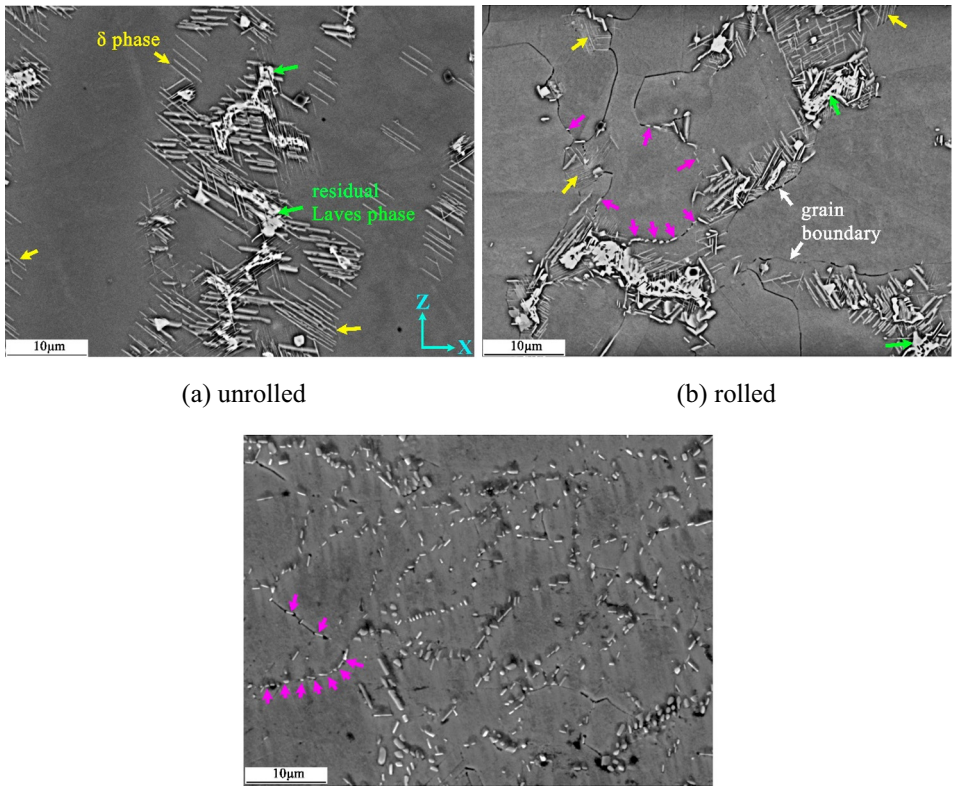


Fig. 12. Precipitates in WAAM and wrought IN718 after solution plus aging.

smaller size, as compared to complete finely equiaxed grains in the wrought alloy. This is due to the unidirectional rolling principle in this study and lack of multiple rolling cycles. On the other hand, the Laves phase forms as a result of the characteristic thermal process in WAAM and still exists in the rolled alloy after solution plus aging treatment, which is not observed in the wrought alloy. Though the present study shows that the non-uniformly recrystallized grains structure and the residual Laves phase has no effect on the room temperature tensile properties, it is not clear whether they could affect other properties, such as creep and rupture strength at high temperatures. In the future, the authors will evaluate the effect of the residual columnar grains and Laves phase on the high-temperature mechanical behaviors; besides, the rolling strategy will be optimized to induce a more complete and uniform recrystallization.

5. Conclusions

With 75 kN interpass rolling applied to WAAM of IN718, the following conclusions can be drawn,

1. The average UTS of the WAMM IN718 is 220 MPa lower than the wrought alloy after heat treatment due to the very large columnar grains.
2. Interpass rolling results in a non-uniform recrystallization; after heat treatment, the average UTS of the rolled WAAM IN718 is 75 MPa higher than the wrought alloy; besides, both 0.2%YS and elongation meet the wrought standard.
3. An effective rolling pass must generate a hardening depth greater than the remelting depth to allow recrystallization to take place upon subsequent depositions.
4. The rolled WAAM IN718 shows better aging response than the unrolled alloy (391 MPa vs. 321 MPa); the overall strengthening (295 MPa) results mainly (76%) from the rolling induced recrystallization.
5. The rolled WAAM IN718 is not microstructurally and metallurgically identical to the wrought alloy; residual Laves phase and numerous δ phase are found in the heat treated condition but their effect are not clear yet.

Acknowledgements

The authors wish to acknowledge the financial support from China Scholarship Council (NO. 201506680057) and the WAAMMat programme industrial partners. The authors would also like to thank Steve Pope, Christine Kimpton, and Tracey Roberts for the assistance during the metallographic and SEM/XRD analysis, and Lisa Blanchard and Kostas Georgilas for their assistance with the EBSD analysis at TWI Ltd. The technical discussion with Dr Paul Colegrove and Dr Jan Honnige, and the assistance from Flemming Nielsen and Nisar Shah during the rolling experiment is much appreciated.

References

[1] D. Zhang, W. Niu, X. Cao, Z. Liu, Effect of standard heat treatment on the microstructure and mechanical properties of selective laser melting manufactured Inconel 718 superalloy, Mater. Sci. Eng. A 644 (2015) 32–40, https://doi.org/10.1016/j.msea.2015.06.021.
[2] B. Baufeld, Mechanical properties of INCONEL 718 parts manufactured by shaped metal deposition (SMD), J. Mater. Eng. Perform. 21 (2012) 1416–1421, https://doi.org/10.1007/s11665-011-0009-y.
[3] H. Qi, M. Azer, A. Ritter, Studies of standard heat treatment effects on microstructure and mechanical properties of laser net shape manufactured INCONEL 718, Metall. Mater. Trans. A 40 (2009) 2410–2422, https://doi.org/10.1007/s11661-009-9949-3.
[4] Y.N. Zhang, X. Cao, P. Wanjara, M. Medraj, Oxide films in laser additive manufactured Inconel 718, Acta Mater. 61 (2013) 6562–6576, https://doi.org/10.1016/j.actamat.2013.07.039.
[5] M. Sundararaman, R. Kishore, P. Mukhopadhyay, Strain hardening in underaged INCONEL 718, Metall. Mater. Trans. A 25 (1994) 653–656, https://doi.org/10.1007/BF02651609.

[6] Special Metals, INCONEL Alloy 7182007 1–28 (doi:SMC-066).
[7] ASM International, ASM Handbook: Volume 2 Properties and Selection: Nonferrous Alloys and Special-purpose Materials, 1990.
[8] D.G. Thakur, B. Ramamoorthy, L. Vijayaraghavan, Effect of cutting parameters on the degree of work hardening and tool life during high-speed machining of Inconel 718, Int. J. Adv. Manuf. Technol. 59 (2012) 483–489, https://doi.org/10.1007/s00170-011-3529-6.
[9] S. Gorsse, C. Hutchinson, M. Gouné, R. Banerjee, Additive manufacturing of metals: a brief review of the characteristic microstructures and properties of steels, Ti-6Al-4V and high-entropy alloys, Sci. Technol. Adv. Mater. 18 (2017) 584–610, https://doi.org/10.1080/14686996.2017.1361305.
[10] T. Trosch, J. Strößner, R. Völkl, U. Glatzel, Microstructure and mechanical properties of selective laser melted Inconel 718 compared to forging and casting, Mater. Lett. 164 (2015) 428–431, https://doi.org/10.1016/j.matlet.2015.10.136.
[11] C. Zhong, A. Gasser, J. Kittel, K. Wissenbach, R. Poprawe, Improvement of material performance of Inconel 718 formed by high deposition-rate laser metal deposition, Mater. Des. 98 (2016) 128–134, https://doi.org/10.1016/j.matdes.2016.03.006.
[12] P.L. Blackwell, The mechanical and microstructural characteristics of laser-deposited IN718, J. Mater. Process. Technol. 170 (2005) 240–246, https://doi.org/10.1016/j.jmatprotec.2005.05.005.
[13] Q. Jia, D. Gu, Selective laser melting additive manufacturing of Inconel 718 superalloy parts: densification, microstructure and properties, J. Alloys Compd. 585 (2014) 713–721, https://doi.org/10.1016/j.jallcom.2013.09.171.
[14] S.W. Williams, F. Martina, A.C. Addison, J. Ding, G. Pardal, P. Colegrove, Wire + arc additive manufacturing, Mater. Sci. Technol. 00 (2015) 1–7, https://doi.org/10.1179/1743284715Y.0000000073.
[15] B. Cong, J. Ding, S. Williams, Effect of arc mode in cold metal transfer process on porosity of additively manufactured Al-6.3%Cu alloy, Int. J. Adv. Manuf. Technol. 76 (2014) 1593–1606, https://doi.org/10.1007/s00170-014-6346-x.
[16] B. Cong, R. Ouyang, B. Qi, J. Ding, Influence of cold metal transfer process and its heat input on weld bead geometry and porosity of aluminum-copper alloy welds, Rare Metal Mater. Eng. 45 (2016) 606–611, https://doi.org/10.1016/S1875-5372(16)30080-7.
[17] B. Wu, Z. Pan, D. Ding, D. Cuiuri, H. Li, Z. Fei, The effects of forced interpass cooling on the material properties of wire arc additively manufactured Ti6Al4V alloy, J. Mater. Process. Technol. 258 (2018) 97–105, https://doi.org/10.1016/j.jmatprotec.2018.03.024.
[18] G. Asala, A.K. Khan, J. Andersson, O.A. Ojo, Microstructural analyses of ATI 718Plus® produced by wire-ARC additive manufacturing process, Metall. Mater. Trans. A Phys. Metall. Mater. Sci. 48 (2017) 4211–4228, https://doi.org/10.1007/s11661-017-4162-2.
[19] D. Clark, M.R. Bache, M.T. Whittaker, Shaped metal deposition of a nickel alloy for aero engine applications, J. Mater. Process. Technol. 203 (2008) 439–448, https://doi.org/10.1016/j.jmatprotec.2007.10.051.
[20] P.A. Colegrove, H.E. Coules, J. Fairman, F. Martina, T. Kashoob, H. Mamash, L.D. Cozzolino, Microstructure and residual stress improvement in wire and arc additively manufactured parts through high-pressure rolling, J. Mater. Process. Technol. 213 (2013) 1782–1791, https://doi.org/10.1016/j.jmatprotec.2013.04.012.
[21] J. Ding, P. Colegrove, F. Martina, S. Williams, R. Wiktorowicz, M.R. Palt, Development of a laminar flow local shielding device for wire + arc additive manufacture, J. Mater. Process. Technol. 226 (2015) 99–105, https://doi.org/10.1016/j.jmatprotec.2015.07.005.
[22] ASTM, ASTM E112-13: Standard Test Methods for Determining Average Grain Size, ASTM Int., 2013 1–28, https://doi.org/10.1520/E0112-13.1.4.
[23] X. Xu, S. Ganguly, J. Ding, S. Guo, S. Williams, F. Martina, Microstructural evolution and mechanical properties of maraging steel produced by wire+arc additive manufacture process, Mater. Charact. (2018)https://doi.org/10.1016/j.matchar.2017.12.002.
[24] P. Kürnsteiner, M.B. Wilms, A. Weisheit, P. Barriobero-Vila, E.A. Jägle, D. Raabe, Massive nanoprecipitation in an Fe-19Ni-xAl maraging steel triggered by the intrinsic heat treatment during laser metal deposition, Acta Mater. 129 (2017) 52–60, https://doi.org/10.1016/j.actamat.2017.02.069.
[25] C. Tan, K. Zhou, W. Ma, P. Zhang, M. Liu, T. Kuang, Microstructural evolution, nanoprecipitation behavior and mechanical properties of selective laser melted high-performance grade 300 maraging steel, Mater. Des. 134 (2017) 23–34, https://doi.org/10.1016/j.matdes.2017.08.026.
[26] E.A. Jägle, P.-P. Choi, J. Van Humbeeck, D. Raabe, Precipitation and austenite reversion behavior of a maraging steel produced by selective laser melting, J. Mater. Res. 29 (2014) 2072–2079, https://doi.org/10.1557/jmr.2014.204.
[27] J. Donoghue, A.A. Antonysamy, F. Martina, P.A. Colegrove, S.W. Williams, P.B. Prangnell, The effectiveness of combining rolling deformation with wire-arc additive manufacture on β-grain refinement and texture modification in Ti-6Al-4V, Mater. Charact. 114 (2016) 103–114, https://doi.org/10.1016/j.matchar.2016.02.001.
[28] F. Martina, P.A. Colegrove, S.W. Williams, J. Meyer, Microstructure of interpass rolled wire + arc additive manufacturing Ti-6Al-4V components, Metall. Mater. Trans. A Phys. Metall. Mater. Sci. 46 (2015) 6103–6118, https://doi.org/10.1007/s11661-015-3172-1.
[29] G.P. Dinda, A.K. Dasgupta, J. Mazumder, Laser aided direct metal deposition of Inconel 625 superalloy: microstructural evolution and thermal stability, Mater. Sci. Eng. A 509 (2009) 98–104, https://doi.org/10.1016/j.msea.2009.01.009.
[30] H. Xiao, S. Li, X. Han, J. Mazumder, L. Song, Laves phase control of Inconel 718 alloy using quasi-continuous-wave laser additive manufacturing, Mater. Des. 122 (2017) 330–339, https://doi.org/10.1016/j.matdes.2017.03.004.
[31] N. Hansen, Hall-petch relation and boundary strengthening, Scr. Mater. 51 (2004) 801–806, https://doi.org/10.1016/j.scriptamat.2004.06.002.



https://dspace.org/

Enhancing mechanical properties of wire+arc additively manufactured INCONEL 718 superalloy through in-process thermomechanical processing

Xu, Xiangfang; Ganguly, Supriyo; Ding, Jialuo; Seow, Cui Er; Williams, Stewart W.

2018-10-27
Elsevier
https://doi.org/10.1016/j.matdes.2018.10.038
Xu X, Ganguly S, Ding J, et al., (2018) Enhancing mechanical properties of wire+arc additively manufactured INCONEL 718 superalloy through in-process thermomechanical processing. Materials and Design, Volume 160, December 2018, pp.1042-1051

Downloaded from a DSpace repository. https://dspace.org/